Journal of Saudi Chemical Society (2019) **23**, 612–626

King Saud University

Journal of Saudi Chemical Society

www.ksu.edu.sa
www.sciencedirect.com

ORIGINAL ARTICLE

Effect of Fe-Mo promoters on HZSM-5 zeolite catalyst for 1-hexene aromatization

Andrii Kostyniuk [a,*], **David Key** [b], **Masikana Mdleleni** [b]

[a] *Department of Catalysis and Chemical Reaction Engineering, National Institute of Chemistry, Hajdrihova 19, Ljubljana 1001, Slovenia*
[b] *PetroSA Synthetic Fuels Innovation Centre, South African Institute for Advanced Materials Chemistry, University of the Western Cape, Cape Town, Private Bag X17, Bellville, 7535, South Africa*

Received 23 May 2018; revised 9 October 2018; accepted 7 November 2018
Available online 15 November 2018

KEYWORDS

HZSM-5;
Fe-Mo species;
Olefins;
Aromatization;
1-Hexene;
Liquid Fuels

Abstract The promotional effect of Fe-Mo species introduced into HZSM-5 (Zeolyst Int., $SiO_2/Al_2O_3 \approx 30$) zeolite catalyst by the wetness impregnation method for the 1-hexene aromatization was investigated. The structure and catalytic performance for the aromatization of 1-hexene over xFeyMo-ZSM-5 catalysts in comparison with unmodified HZSM-5 catalysts were studied. The xFeyMo-ZSM-5 catalysts contain fixed loading (5 wt%) and variable Fe/Mo ratio. The catalysts were characterized by BET, ICP-AES, HRSEM-EDS, HRTEM, XRD, FTIR, H_2-TPR, NH_3-TPD, and pyridine DRIFT spectroscopy. The characterization data confirmed the existence of Fe and Mo species in the zeolite matrix. With Fe and Mo species implementation to HZSM-5 zeolite, the amount of the acid sites decreased, but the selectivities to C_{9+} aromatics increased. The catalyst evaluation was performed at 350 °C for 6 h on-stream at atmospheric pressure using a fixed-bed quartz tube reactor. The selectivity to products of different carbon number was affected by the Fe/Mo ratio within the zeolite. It was found the product distribution of grouped fractions of C_1–C_{17+} from the liquid product. The results indicate that the optimum ratio of Fe/Mo is 1–1.5. The highest selectivity for gasoline and distillate ranges was obtained for the 2.5wt%Fe2.5wt% Mo- and 3wt%Fe2wt%Mo-ZSM-5 samples, which was higher than that for parent HZSM-5 catalyst.

1. Introduction

An important industrial way for the olefins upgrading is the aromatization and skeletal hydroisomerization of olefins over acid catalyst [1–6]. It is well-known that the aromatization of olefins has great significance in the chemical industrial fields for synthetic resin, rubber, solvent, detergent, clean gasoline and other chemical intermediates [5]. The most investigated olefins are propene and butene using phosphoric impregnated

* Corresponding author.
E-mail addresses: andry_kost@ukr.net (A. Kostyniuk), dkey@uwc.ac.za (D. Key), masikana.mdleleni@petrosa.co.za (M. Mdleleni).
Peer review under responsibility of King Saud University.

Production and hosting by Elsevier

https://doi.org/10.1016/j.jscs.2018.11.001
1319-6103

silica–clay acid and zeolite type of catalysts [7–11], but studies dealing with 1-hexene transformation are consequently limited [12]. The products of this process are mixtures of olefins, straight chain paraffins, cycloalkanes, and aromatics which are contained in gasoline (C_5–C_{10}) and diesel (C_{10}–C_{20}) [10,11]. 1-hexene aromatization can undergo many reactions over the zeolites, such as cracking, oligomerization, isomerization, cyclization, as well as hydrogen transfer over the Brønsted and Lewis acid sites of the zeolite [5,6]. In general, low temperatures (250 °C) favored the double bond shift reaction but for the cracking is the major reaction at temperatures above 450 °C [6]. The balanced aromatization and hydroisomerization reactions at moderate temperatures among 300–400 °C appear to be attractive for achieving the desired RON (research octane number) and gasoline yield simultaneously in the olefins upgrading [1].

Zeolite catalysts are widely uses for aromatization of olefins [8,10,13]. ZSM-5 zeolite is one of the best solid acid catalysts and has been widely applied in petrochemical industry, due to its unique structures, thermal stability, acidity and shape selectivity [1,2,14]. Many researchers studied the aromatization process over ZSM-5 modified by Pt, Ga, and Zn, with the goal of reducing coke formation, which leads to rapid catalyst deactivation and poor stability [3–6]. In addition, the strength of acid sites in promoted zeolite catalysts, which can catalyze the aromatization of olefins, is still unclear. Nevertheless, the results of these investigations suggest that the development of a more active catalyst for aromatization of 1-hexene is needed and still remains a major problem [3,15].

In this paper, the aim of this study was to prepare and investigate Fe-Mo bimetal zeolite catalysts and study the effect of adding metal species for the 1-hexene aromatization, which has never been reported before. For such a purpose, Fe-Mo species were incorporated into HZSM-5 zeolite by the wetness impregnation method and can be used to enhance zeolite activity during the 1-hexene aromatization. The effects of Fe/Mo ratio on the catalysts activity and product distribution will be evaluated.

2. Experimental

2.1. Chemicals used

Reagents that have been used in the preparation of the catalyst and the catalytic reaction: NH_4-ZSM-5 zeolite (Zeolyst Int., CBV 3024E), iron(III) nitrate nonahydrate (Sigma-Aldrich, ≥98%), ammonium heptamolybdate tetrahydrate (Sigma-Aldrich, 99.98%), 1-hexene (Sigma-Aldrich, 97%).

2.2. Catalyst synthesis

The preparation of the xFeyMo-ZSM-5 catalysts has involved the impregnation of the commercial NH_4-ZSM-5 zeolite (SiO_2/$Al_2O_3 \approx 30$) using the incipient wetness impregnation method with solutions of ammonium heptamolybdate $(NH_4)_6Mo_7O_{24}\cdot 4H_2O$ and iron(III) nitrate $Fe(NO_3)_3\cdot 9H_2O$. At first, the NH_4-ZSM-5 zeolite was calcined at 550 °C in static air for 6 h to convert the ammonium form to its protonated form (H-ZSM-5). Samples containing both molybdenum and iron were prepared by a two-step impregnation procedure, in which the molybdenum phase with a concentration of 0.001 M was introduced first to the H-ZSM-5 and mixed for 2 h at 80 °C. After that, the iron salt with a concentration of 0.01 M was added to the prepared solution with vigorous stirring. The temperature was kept at 80 °C. Stirring continued until suspension turned into a slurry. Drying was carried out at 120 °C in the ventilated dryer overnight. Thereafter calcination in the static air was carried out for 6 h at 550 °C. 10 different catalysts based on H-ZSM-5 were prepared in this way with the following amounts of metals: 5wt%Mo, 1wt%Fe4wt%Mo, 1.25wt%Fe3.75wt%Mo, 1.43wt%Fe3.57wt%Mo, 1.67wt%Fe3.33wt%Mo, 2wt%Fe3wt%Mo, 2.5wt%Fe2.5wt%Mo, 3wt%Fe2wt%Mo, 4wt%Fe1wt%Mo and 5wt%Mo. All percentages associated with metal amount are expressed as weight percentage.

2.3. Catalyst characterization

2.3.1. Fourier transform infrared (FT-IR) spectroscopy analysis

The FTIR framework spectra were obtained using Perkin Elmer UATR FTIR spectrometer. Typically 20 mg of sample was placed on the ATR diamond crystal and the force gauge set to 50 (arb. units) to obtain good contact between sample and crystal. The samples were recorded in the region 400 to 4000 cm^{-1}.

2.3.2. Surface area and micropore analysis (BET)

Brunauer–Emmett–Teller (BET) specific surface area was determined using a Micrometrics 3300, TriStar surface area and porosity analyzer. About 0.3 g of sample was degassed at 400 °C for 4 h. After the degassing process, the samples were then loaded on the analysis station for determination of the isotherms at −196 °C. The pore size distributions were calculated using the Barrett–Joyner–Halenda (BJH) model applied to the adsorption branch of the isotherm, assuming cylindrical pore geometry.

2.3.3. ICP-AES analysis

The chemical analysis of elements' (Fe and Mo) amount in catalysts was determined by inductively coupled plasma atomic emission spectroscopy (ICP-AES) on Varian model 715-ES. Prior to the ICP-AES measurements, the zeolite samples were dissolved in a mixture of $HF/HNO_3/H_2O$ (1:1:1).

2.3.4. HRSEM-EDS analysis

Scanning electron microscopy (SEM) micrographs were obtained using a high-resolution SEM EHT 5.00 kV. All samples were carbon coated before imaging. The HRSEM (AURIGA) was also equipped with an EDS spectrometer with the INCA EDS system by Oxford Instruments for elemental analysis of zeolites.

2.3.5. HRTEM analysis

Transmission electron microscopy images were obtained using the aid of HRTEM techniques using a FEI Tecnai TF20 (200 kV) equipped with a STEM unit, high-angle annular dark-field (HAADF) detector and X-Twin lenses.

2.3.6. Powder X-ray diffraction analysis

Powder X-ray diffraction data were collected using a Brucker AXS D8 diffractometer equipped with a primary beam Gobel

mirror, a radial Soller slit, a Vantec-1 detector and using Cu-Kα radiation (40 kV, 40 mA, λKα1 = 1.5406 Å). Data were collected in the 2θ range 5 to 70° and 90° in 0.021° steps, using a scan speed resulting in an equivalent counting time of 14.7 s/step.

2.3.7. H_2-TPR analysis

Temperature programmed reduction (TPR) characteristics of the catalysts were obtained using a Micrometrics Autochem 2920 II system. Sample (0.1 g) was loaded in a U-shaped quartz tubular reactor. When performing the TPR analysis, the sample was exposed to a gas mixture (10% H_2, balance Ar) at a flow rate of 50 mL/min and heated to 900 °C at 10 °C/min heating rate. The H_2 consumption was monitored with a thermal conductivity detector (TCD). A cooling trap (ice + isopropanol) placed between the sample and the TCD was used to retain the water produced during the reduction process.

2.3.8. NH_3-TPD analysis

The acid properties of the catalysts were determined by temperature-programmed desorption of ammonia (NH_3-TPD) on a Micrometrics Autochem 2920 II system using He as a carrier gas. All samples (0.1 g) were first heated to 500 °C and then cooled down to 120 °C in He atmosphere. Afterward, 5 vol% NH_3 in He (20 mL/min) was adsorbed at 120 °C for 30 min followed by He purging at the same temperature for 1 h. Desorption of NH_3 was monitored in the range of 120–700 °C at a 10 °C/min heating rate. The NH_3 desorption profile was observed using a thermal conductivity detector.

2.3.9. Pyridine-DRIFT analysis

Thermogravimetric method of pyridine adsorption was used for quantification of acid sites on investigated materials using Pyris 1 TGA apparatus from PerkinElmer. Prior to analysis, the samples were degassed *in-situ* in N_2 stream (30 mL/min) at 500 °C for 1 h. Afterward, the sample was cooled to 125 °C and saturated with pyridine vapors by passing the N_2 stream through a saturator filled with liquid pyridine. Saturation was followed by desorption of weakly bound pyridine by degassing the sample in N_2 at 125 °C for an additional 2 h until achieving a stable sample weight. The total number of acid sites was calculated based on the weight difference before and after sample saturation.

Differentiation between Brønsted (BAS) and Lewis (LAS) acid sites was done for pure HZSM-5 and 2.5Fe2.5Mo-HZSM-5 materials by DRIFTS analysis using Frontier IR spectrometer (Perkin Elmer), DiffusIR® accessory from Pike Scientific and pyridine as the probe molecule. The powdered samples (~10 mg) were positioned in the sample cup and pretreated in N_2 (50 mL/min) at 500 °C for 30 min. After cooling to 125 °C, the samples were saturated with pyridine vapors for 10 min, followed by degassing in a vacuum (2×10^{-5} mbar) for 30 min. Spectra were recorded with 8 accumulations and spectral resolution of 4 nm between 800 and 4000 cm^{-1}. For characterization of LAS and BAS, absorption bands at 1445 cm^{-1} and 1545 cm^{-1} were considered.

2.4. Catalytic evaluation

The performances of the zeolite catalysts were tested in the conversion of 1-hexene in a fixed bed quartz tube reactor at a weight hourly space velocity (WHSV) of 4 h^{-1} and the reaction temperature was kept at 350 °C under atmospheric pressure. The reactor tube was charged with 1 g of a catalyst then heated from room temperature up to 350 °C. 1-hexene was introduced by New era syringe pump at a flow rate of 0.098 mL/min with the syringe of 29 mm diameter continuously for 6 h. All products were analyzed on an offline Bruker 450 GC equipped with a BR-Alumina/Na_2SO_4 column (C_1–C_6), BR-1 column (C_7–C_{17}) and a flame ionization (FID) detector. 1-hexene conversion and selectivity were defined as:

$$X_{1-\text{hexene}}(\text{mol}\%) = \frac{(\text{1-hexene moles in the feed}) - (\text{1-hexene moles in the products})}{(\text{1-hexene moles in the feed})}$$

$$S_{\text{CxHy}}(\text{mol}\%) = \frac{\text{CxHy moles in the products}}{\sum \text{CxHy moles in the products}} \times 100$$

3. Results and discussion

3.1. Catalyst characterization

3.1.1. Surface area and micropore analysis (BET)

Table 1 summarizes the nominal composition of samples with different Mo/Fe ratio and fixed loading (5wt%). The BET surface area (S_{BET}), microporous surface area (S_{micro}), external surface area (S_{extrer}), microporous volume (V_{micro}), total pore volume (V_{total}), average pore diameters and hierarchy factor (HF) of the studied catalysts are listed in Table 2 [16].

Correspondingly, the micropore volume of promoted HZSM-5 zeolite was reduced from 0.105 to 0.094 cm^3/g, as revealed in Table 2. After loading 5wt% of Mo on HZSM-5, the S_{BET} decreased from 378 to 314 cm^2/g due to strong Mo interaction with HZSM-5 and indicating that Mo mostly deposited on the external surfaces and could have blocked some of the micropores of HZSM-5 [16–18]. Upon addition

Table 1 Nominal composition for prepared samples of xFeyMo-ZSM-5 catalysts.

Sample	xFe (wt%)	yMo (wt %)	Mo/Fe ratio	Total load (wt%)
Fixed loading and variable Mo/Fe ratio				
5Mo	0	5	∞	5
1Fe4Mo	1	4	4	5
1.25Fe3.75Mo	1.25	3.75	3	5
1.43Fe3.57Mo	1.43	3.57	2.5	5
1.67Fe3.33Mo	1.67	3.33	2	5
2Fe3Mo	2	3	3/2	5
2.5Fe2.5Mo	2.5	2.5	1	5
3Fe2Mo	3	2	2/3	5
4Fe1Mo	4	1	1/4	5
5Fe	5	0	0	5

Table 2 Characterization data of the zeolite samples.

Catalyst	Fe[a] (wt%)	Mo[a] (wt%)	S_{BET}[b] (m^2/g)	S_{micro}[b] (m^2/g)	S_{exter}[b] (m^2/g)	V_{micro}[c] (cm^3/g)	V_{total}[c] (cm^3/g)	BJH Adsorption average pore diameter[d] (nm)	BJH Desorption average pore diameter[d] (nm)	HF
HZSM-5	–	–	378	228	150	0.105	0.235	5.92	5.75	0.178
5Mo	–	4.74	314	207	107	0.096	0.208	6.13	5.81	0.158
1Fe4Mo	0.92	3.82	326	203	123	0.094	0.215	6.24	5.95	0.165
1.25Fe3.75Mo	1.13	3.65	330	205	125	0.095	0.218	5.73	5.50	0.165
1.43Fe3.57Mo	1.40	3.46	324	204	120	0.095	0.211	5.56	5.31	0.167
1.67Fe3.33Mo	1.61	3.10	339	207	132	0.096	0.223	5.67	5.48	0.168
2Fe3Mo	1.94	2.85	316	203	113	0.094	0.210	6.83	4.41	0.161
2.5Fe2.5Mo	2.47	2.36	331	204	127	0.094	0.221	6.01	5.75	0.164
3Fe2Mo	2.91	1.89	339	217	122	0.100	0.222	5.82	5.60	0.162
4Fe1Mo	3.88	0.89	348	212	136	0.098	0.230	5.82	5.62	0.167
5Fe	4.78	–	346	209	137	0.097	0.228	5.89	5.68	0.168

[a] ICP-AES.
[b] BET method.
[c] t-Plot method.
[d] BJH method.

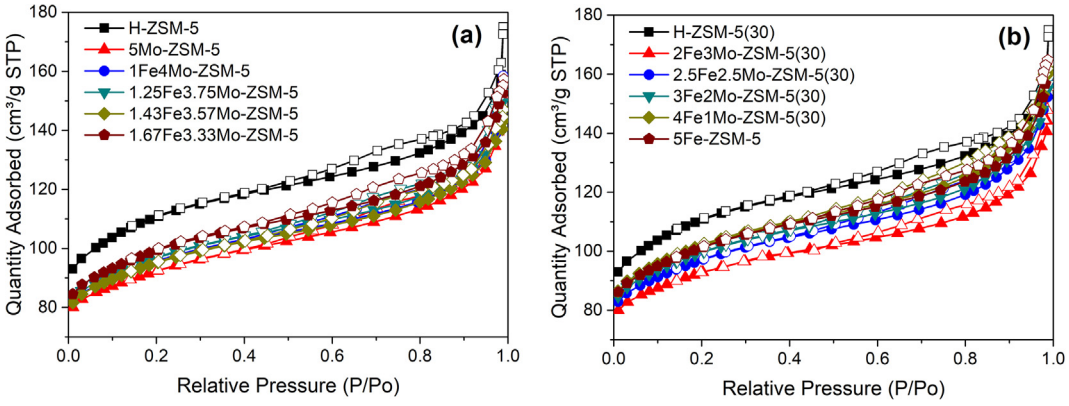

Fig. 1 N_2-adsorption and desorption isotherms (a, b, c) and BJH pore size distribution (d) of the H-ZSM-5 and xFeyMo-ZSM-5 samples.

of 5wt% of Fe the S_{BET} decreased to 346, but not so dramatically comparing with 5wt%Mo.

The xFeyMo-ZSM-5 samples noticed a different behavior with variable Mo/Fe ratio. The xFeyMo-ZSM-5 samples exhibit a greater surface area than 5Mo-ZSM-5 suggesting a better dispersion when Fe and Mo metals are both present [16,18].

Fig. 1(a, b, c) provides the N_2 adsorption-desorption isotherms for samples with different Mo/Fe ratio. The characteristic of the xFeyMo-ZSM-5 samples tending to agglomerate into microsized agglomerates is also featured by its N_2 adsorption and desorption isotherms, which could also be supported by the XRD and SEM results [17]. As shown in Fig. 1 all catalysts exhibit typical type I isotherms with a small hysteresis loop in the range of $p/p^0 = 0.5–0.9$, which indicate that the HZSM-5 and xFeyMo-ZSM-5 samples have high microporosity and inter-crystal mesoporosity possibly related to the aggregation of the crystals [3,17,19–22].

Compared with the isotherm of the HZSM-5, for the xFeyMo-ZSM-5 samples, the N_2 adsorption decreased. A little difference in the shape of N_2 adsorption/desorption isotherms for xFeyMo-ZSM-5 samples was observed, but the presence of both Fe and Mo on the external surfaces of zeolite crystals has little influence on their agglomeration behaviors [17].

The hierarchy factor (HF) can be applied to any material, to classify the porous characteristic [23,24]. The hierarchy factors were calculated according to Eq. (1).

$$HF = (S_{exter}/S_{BET}) \times (V_{micro}/V_{total}) \quad (1)$$

Well-known conventional zeolites display moderate HF value (≤ 0.1) and hierarchical zeolites display relatively high HF value (> 0.1) due to the introduction of mesopores. The HF value of the metals promoted and parent ZSM-5 is 0.158–0.178 (> 0.1), that is, displaying high relative mesoporosity, in good agreement with the TEM images [23].

The pore size distribution was obtained by applying the Barrett–Joyner–Halenda (BJH) method from the adsorption branches of nitrogen isotherms [25]. Fig. 1d shows the mesopores with sizes in a range of 12.5–21.0 nm [3]. The majority of these pores concentrated at about 14 nm. Compared with HZSM-5 catalyst, there was a notable increase in the pore size distribution for the 2.5Fe2.5Mo-ZSM-5 (14.5 nm), 3Fe2Mo-ZSM-5 (14.5 nm), 4Fe1Mo-ZSM-5 (12.5 nm) and 5Fe-ZSM-5 (21.0 nm) samples, exhibiting that the increase in incorporation of Fe-Mo species in the framework made the pore diameter larger. Thus, impregnation does not change the

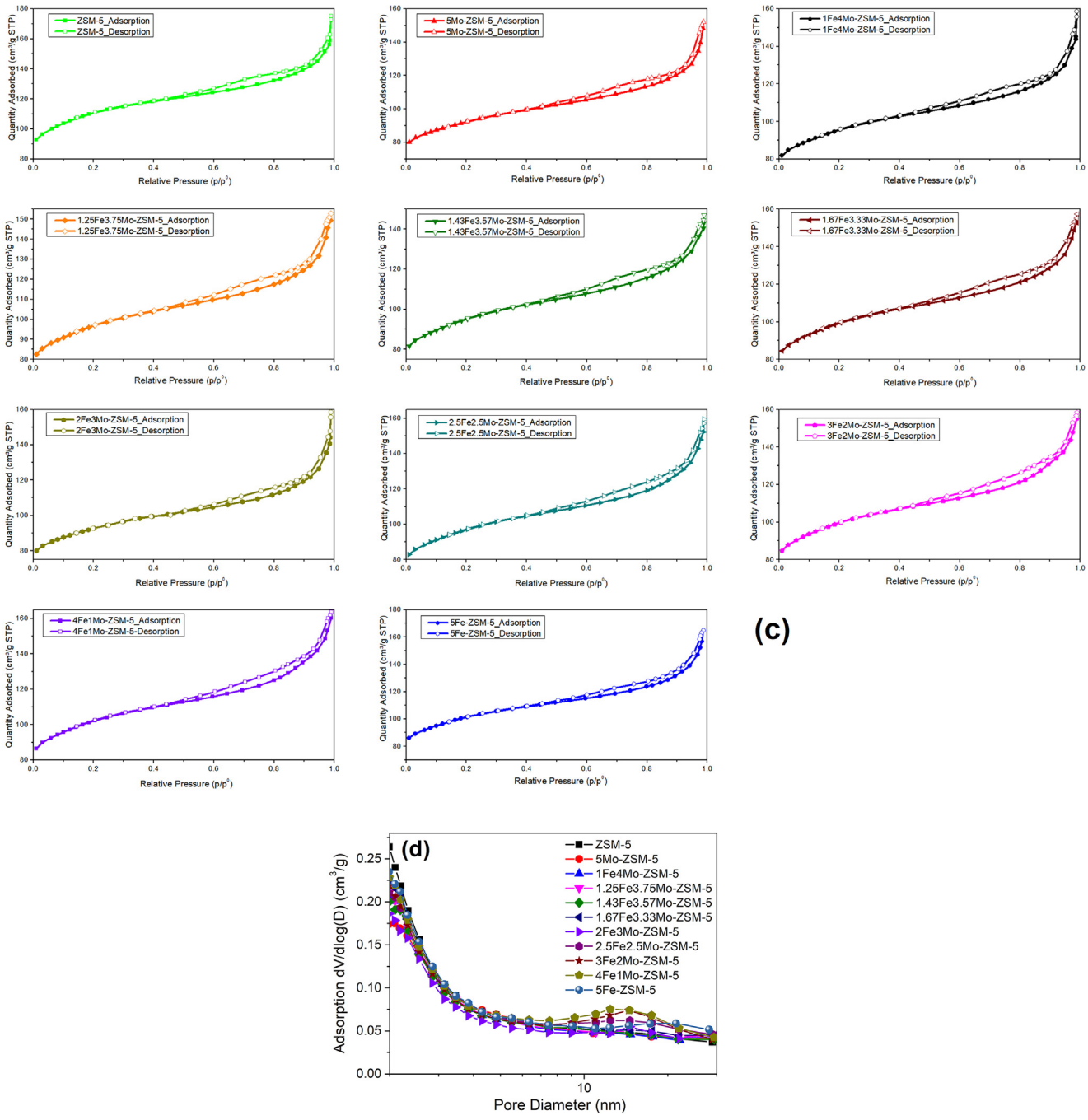

Fig. 1 (*continued*)

texture of catalysts which agrees with XRD, FTIR, SEM and TEM results [26].

3.1.2. Electron microscopy and X-ray microanalysis

The HRSEM-EDS images of the HZSM-5 and xFeyMo-ZSM-5 zeolite catalysts are shown in Fig. 2.

The SEM images showed aggregates of particles. No major morphological differences were observed between zeolite catalysts. Fig. 2 shows two typical SEM images obtained. It is clear from the images that the zeolite catalysts have a cube or elongated prismatic shapes [16,17,19,20].

The element mapping of the HZSM-5, 5Fe-ZSM-5, 5Mo-ZSM-5 and 2.5Fe2.5Mo-ZSM-5 samples by HRSEM is shown in Fig. 3.

From Fig. 3 we can see that the distribution of the element Fe and Mo the same as Si and Al is homogeneous. The element analysis shows that the O–K, Al–K, Si–K, Fe–K, Fe–L, Mo–K and Mo–L signals display the elements are uniformly distributed. In other words, the iron and molybdenum species

are well dispersed on the external surface of the HZSM-5 crystals [27].

3.1.3. The high-resolution transmission electron microscopy (HRTEM)

HRTEM and Energy Dispersive Spectroscopy (EDS) were performed for the HZSM-5 and xFeyMo-ZSM-5 samples to confirm the presence of iron and molybdenum species in HZSM-5 and study the composition of the metallic phase in the catalysts. Fig. 4 shows brightfield TEM images. The presence of Fe and Mo particles in these objects is also evidenced by EDS analysis, as it is shown in Fig. 5, where the peaks corresponding to O–K, Al–K, Si–K, Fe–K, Fe–L, Mo–K and Mo–L emissions are clearly outlined together with other peaks that arise from the carbon and the copper grid [28,29]. As it is seen from EDS spot area the Fe and Mo were always detected together and involved in the formation of iron and molybdenum species in the HZSM-5 zeolite catalyst [17].

3.1.4. Fourier transform infrared (FT-IR) measurements

The FT-IR spectra of the HZSM-5 and xFeyMo-ZSM-5 samples were recorded in the range of 4000–400 cm^{-1} and shown in Fig. 6. The absorption bands at 1220, 1075, 797, 542, 433 cm^{-1} are considered as the characteristic signals for the framework vibration of the HZSM-5 zeolite catalyst [30]. It was found that the band 433 cm^{-1} belongs to the T–O bending vibration of internal tetrahedral (where T = Si or Al), 542 cm^{-1} (double ring), 797 cm^{-1} (external symmetric stretch), 1075 cm^{-1} (internal asymmetric stretch) and 1220 cm^{-1} (external asymmetric stretch), respectively [26,30–32].

According to the IR spectra recorded from the xFeyMo-ZSM-5 samples, all the structure-sensitive bands are similar

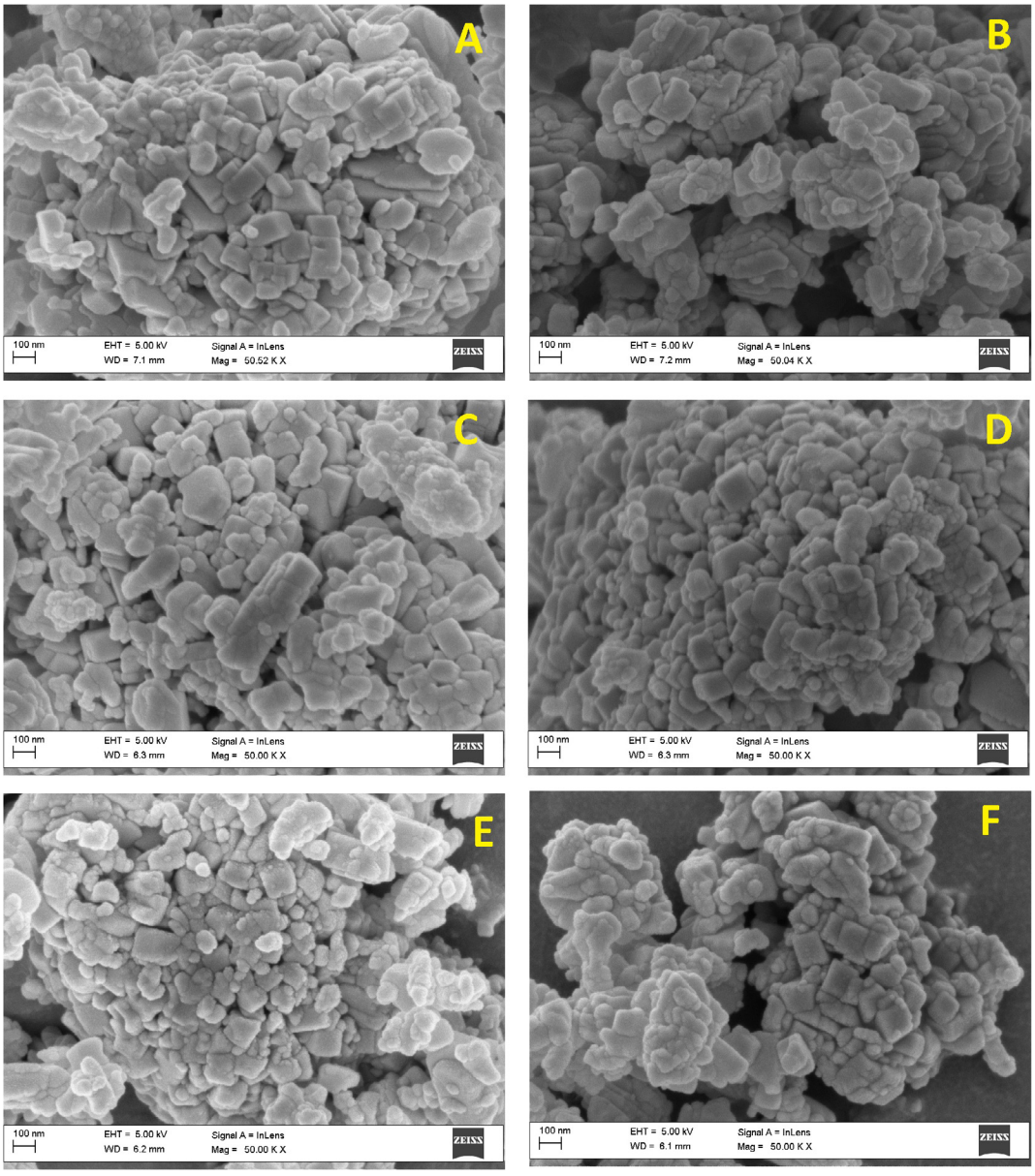

Fig. 2 SEM images of the HZSM-5 and xFeyMo-ZSM-5 samples with fixed loading and variable Mo/Fe ratio (A – HZSM-5, B – 5Mo, C – 1Fe4Mo, D – 1.25Fe3.75Mo, E – 1.43Fe3.57Mo, F – 1.67Fe3.33Mo, G – 2Fe3Mo, H – 2.5Fe2.5Mo, I – 3Fe2Mo, J – 4Fe1Mo, K – 5Fe).

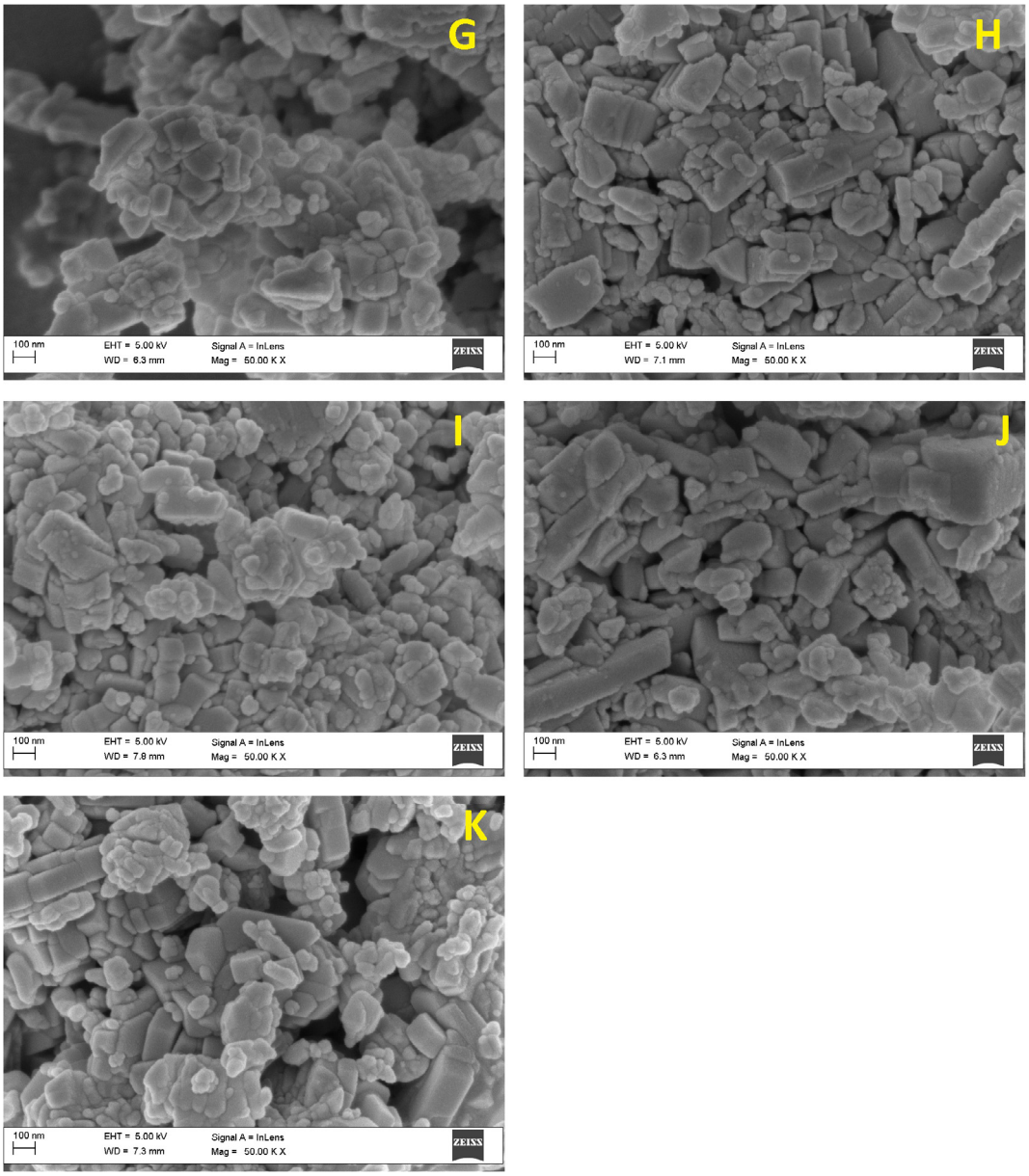

Fig. 2 (*continued*)

to those of HZSM-5, but for the 5Mo-ZSM-5 catalyst, a new band was found.

The spectrum of xFeyMo-ZSM-5 catalysts shows major changes in the region of 750–1000 cm^{-1}, weakening of strong absorption of the band at 797 cm^{-1}. A new broad band was found at 901 cm^{-1}, which corresponds to the overlap between Mo-O-Mo bond vibrations in MoO_3. The band at 1075 cm^{-1} is sensitive to the ratio of framework Si/Al. By the loading of Fe and Mo species, the band at 1075 cm^{-1} shifted to 1081 cm^{-1} (Fig. 6). Thus, the FTIR spectra of HZSM-5 were not significantly affected after loading the Fe and Mo species, which means the introduction of these species did not change the HZSM-5 basic framework [33].

3.1.5. X-ray diffraction (XRD) analysis

Figs. 7-8 shows the XRD patterns of samples with different Fe/Mo ratios. The similarity between the XRD patterns of the HZSM-5 and xFeyMo-ZSM-5 samples indicates that the HZSM-5 framework was preserved after impregnation [16,27,34,35]. In contrast, the samples impregnated with pure Fe, Mo, and Fe-Mo species do not exhibit any reflections related to the iron and molybdenum species indicating very small particles size [30]. As shown in Figs. 7, 8 the Fe-Mo additives cause a decrease in the HZSM-5 crystallinity since a reduction of the HZSM-5 characteristic peaks are observed.

Once all the samples compared with HZSM-5 exhibited a decrease in the peaks between $2\theta = 7.6°–9.2°$ and $2\theta = 22°–29°$, it is reasonable to suppose that the dispersion of iron and molybdenum species takes place on the HZSM-5 surface as well as inside the channels.

3.1.6. H_2–TPR analysis

H_2–TPR experiments were conducted to investigate the reducibility of the metals modified H-ZSM-5 catalysts. In

Fig. 9, the temperature programmed reduction profiles for Fe, Mo and Fe-Mo loaded catalysts are shown. The catalysts exhibit different temperature-programmed reduction profiles indicating the different interaction between active phases [36]. H_2-TPR of unmodified H-ZSM-5 did not show hydrogen consumption in the investigated temperature range [37]. The main reduction peaks corresponding to the metal phase reduction were located between 305 °C and 731 °C. The addition of Mo species in the supported Fe oxide catalyst system shifted the H_2-TPR peaks to higher reduction temperatures, showing the α H_2-TPR peak at 426 °C for the 2.5Fe2.5Mo-ZSM-5 sample [38].

In Fig. 9, three reduction peaks arising from the 2.5Fe2.5Mo-ZSM-5 catalyst can be distinct, the one at 426 °C shows a reduction of Fe_2O_3 to Fe_3O_4, and the others at 523 and 731 °C reduction of Fe_3O_4 to FeO and Fe and interaction with Mo specious [37,39,40].

For the 5Mo-ZSM-5, the H_2 consumption curve deviates from the baseline at approximately 300 °C, and the H_2-TPR peak occurred at above 429, 485 and 668 °C [38]. The peak at 429 and 485 °C is attributed to the reduction of the species Mo^{+6} to Mo^{+4}, from the MoO_3 polymeric species. The peak at 668 °C is assigned to the reduction of the Mo^{2+} phase to Mo^0 [28]. The H_2-TPR curve for the 5Fe-ZSM-5 sample also showing three peaks at 305, 475 and 598 °C with involving the reduction of the iron oxide in a three-step reduction process: $Fe_2O_3 \rightarrow Fe_3O_4 \rightarrow FeO \rightarrow Fe$, respectively.

3.1.7. NH_3-TPD analysis

The concentration and strength of acid sites in HZSM-5 and 2.5Fe2.5Mo-ZSM-5 are determined by NH_3-TPD, as presented in Fig. 10 and the quantitative result is listed in Table 3.

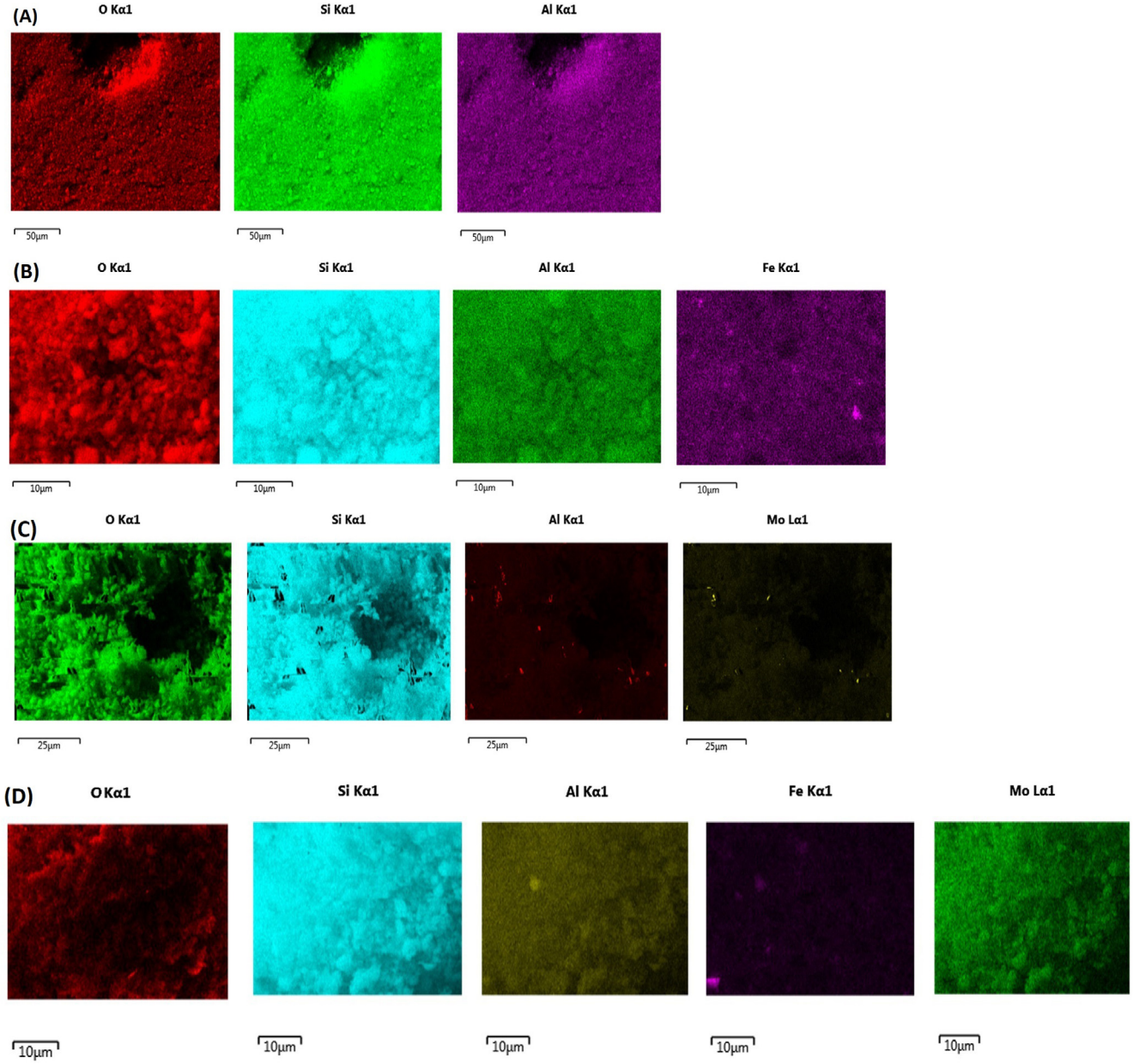

Fig. 3 Element mapping of the HZSM-5 (A), 5Fe-ZSM-5 (B), 5Mo-ZSM-5 (C), 2.5Fe2.5Mo-ZSM-5 (D).

Two desorption peaks were observed for the parent HZSM-5 at 191 and 389 °C. The peak at 191 °C has been assigned to desorption of the absorbed NH_3 on a weak acid (mostly Lewis-acid) sites, whereas, the peak at 389 °C was assigned to medium strong acid (mostly Bronsted-acid) sites [16,27,41]. With the Fe and Mo species were implemented, the area of weak and strong acidic sites decreased [42]. The strong acid sites change more than the weak ones. At the same time, the 2.5Fe2.5Mo-ZSM-5 sample showed NH_3-TPD peaks with lower desorption temperatures in comparison with that of the parent HZSM-5 zeolite. The 2.5Fe2.5Mo-ZSM-5 exhibits obviously weaker acidity than the HZSM-5 catalyst.

The decrease in the amount of strong acid sites results in a decrease in the selectivities to benzene and toluene and an increase in the selectivity to C_{9+} aromatics [42]. The surface acid sites, especially strong acid sites, facilitated the second

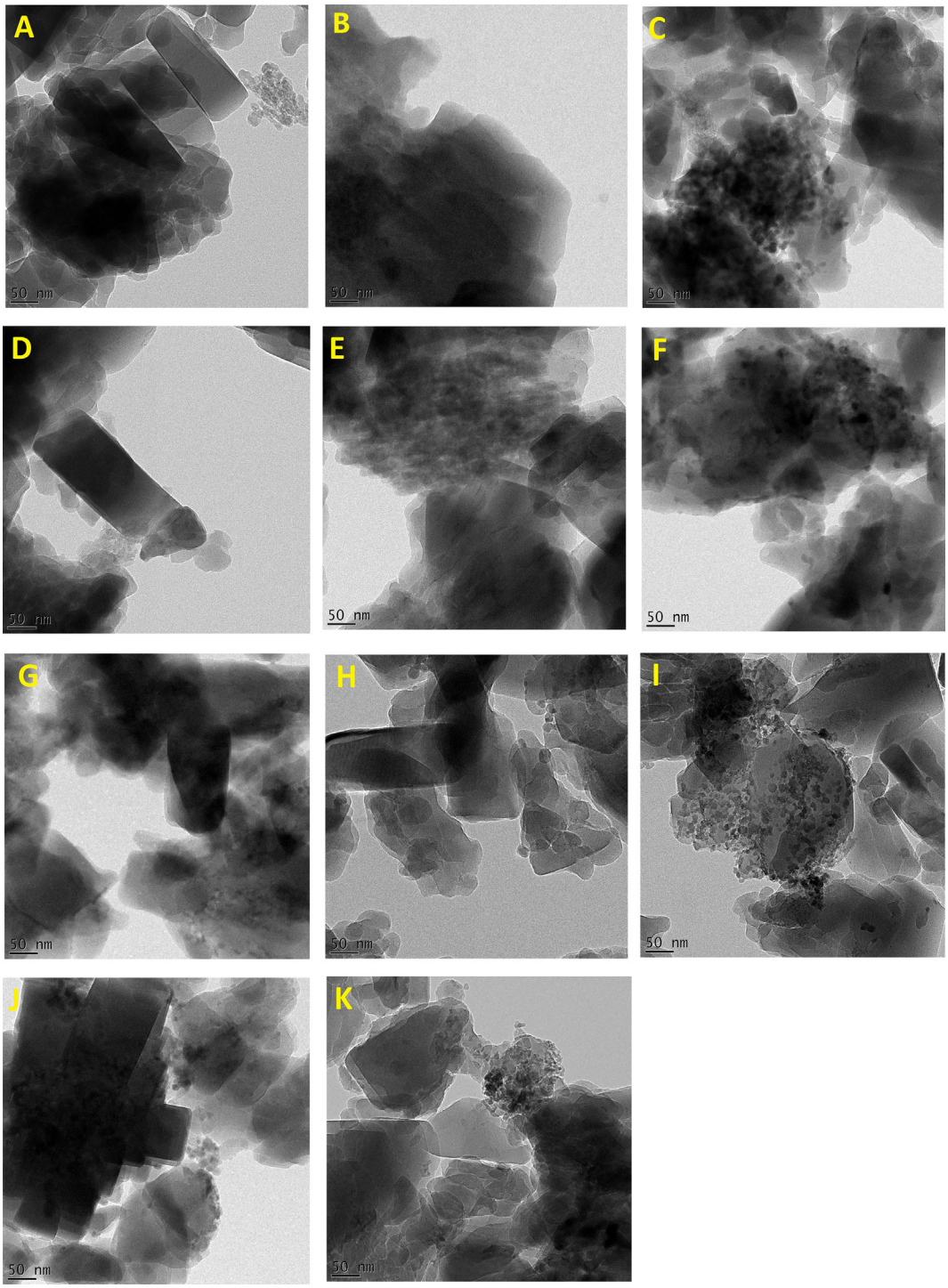

Fig. 4 HRTEM images of the xFeyMo-ZSM-5 catalysts with fixed loading and variable Mo/Fe ratio (A – HZSM-5, B – 5Mo, C – 1Fe4Mo, D – 1.25Fe3.75Mo, E – 1.43Fe3.57Mo, F – 1.67Fe3.33Mo, G – 2Fe3Mo, H – 2.5Fe2.5Mo, I – 3Fe2Mo, J – 4Fe1Mo, K – 5Fe).

reaction of products and coke formation. Therefore, the distinct surface acid strength and acid site density may lead to different catalytic activities of the 2.5Fe2.5Mo-ZSM-5 catalyst for the 1-hexene aromatization reaction [38,43].

3.1.8. Pyridine-DRIFT analysis

For characterization of LAS and BAS, absorption bands at 1445 cm^{-1} and 1545 cm^{-1} were considered. The first band originates from pyridine coordinative adsorbed on LAS, while the second arises from pyridinium ion bound to BAS. The BAS/LAS ratio was calculated as:

$$C_{BAS}/C_{LAS} = 1.73/1.23 \times I_{BAS}/I_{LAS}$$

In this equation, I_{BAS} and I_{LAS} represent the intensity of absorption bands at 1545 and 1445 cm^{-1}, and 1.73 and 1.23 are relevant extinction coefficients, as reported by Tamura et al. [44]. When Fe-Mo species were deposited over HZSM-5, the amount of acid sites decreases slightly, from 0.63 to 0.58 mmol/g_{cat}. This could be connected either to pore blockage and inaccessibility of acid sites to the pyridine probe molecule what was verified by N_2 physisorption. On a side note, the total amount of acid sites assuming all framework Al^{3+} is 1.08 mmol/g. Notably less was measured, suggesting inaccessibility of all acid sites for the probe molecule.

Pyridine DRIFT analysis showed that pure HZSM-5 contains mainly BAS (BAS/LAS = 4). A notable fraction (20%) of aluminum appears as LAS, which suggests their extra-framework location. After Fe-Mo species deposition, a notable increase in LAS is observed (BAS/LAS = 2.7, Table 4). Based on this, the addition of Mo species enhanced the surface weak acid strength in the 2.5Fe2.5Mo-ZSM-5 catalyst [38]. This is anticipated since coordinatively unsaturated Mo^{6+} in MoO_x clusters can exhibit Lewis acidic character.

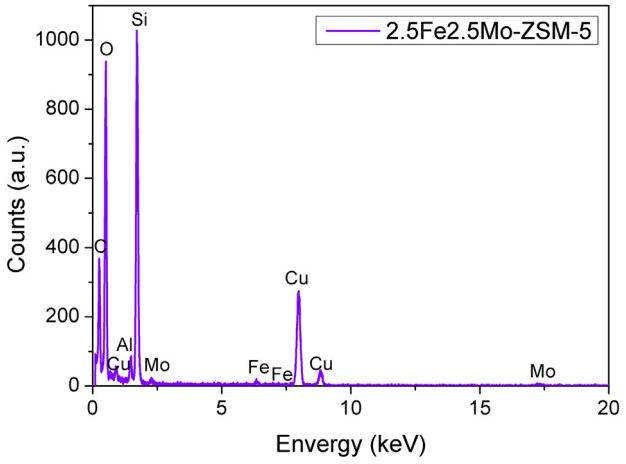

Fig. 5 A typical Energy Dispersive Spectrum (EDS) of the 2.5Fe2.5Mo-ZSM-5 sample.

3.2. Catalyst evaluation

The effect of Fe/Mo ratio on the catalytic conversion of 1-hexene was studied at a reaction temperature of 350 °C for 6 h on-stream. The reaction was performed at atmospheric pressure. The conversion of 1-hexene was observed 99% over

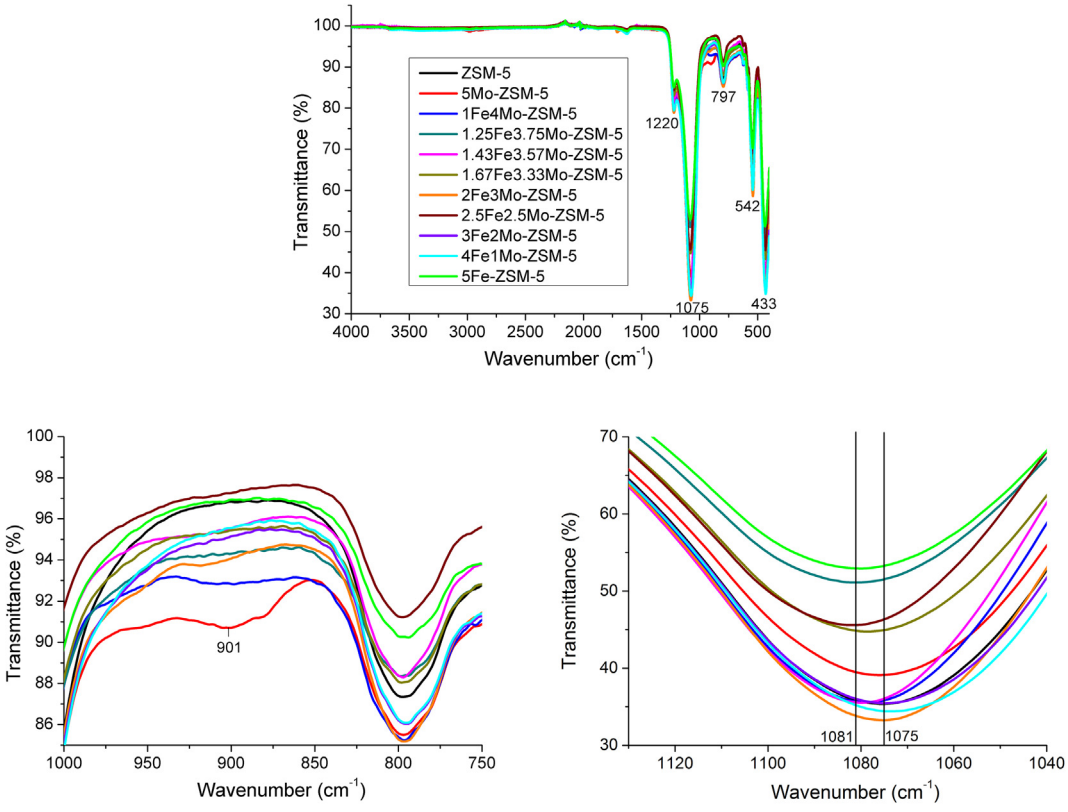

Fig. 6 FT-IR spectra of the HZSM-5 and xFeyMo-ZSM-5 catalysts.

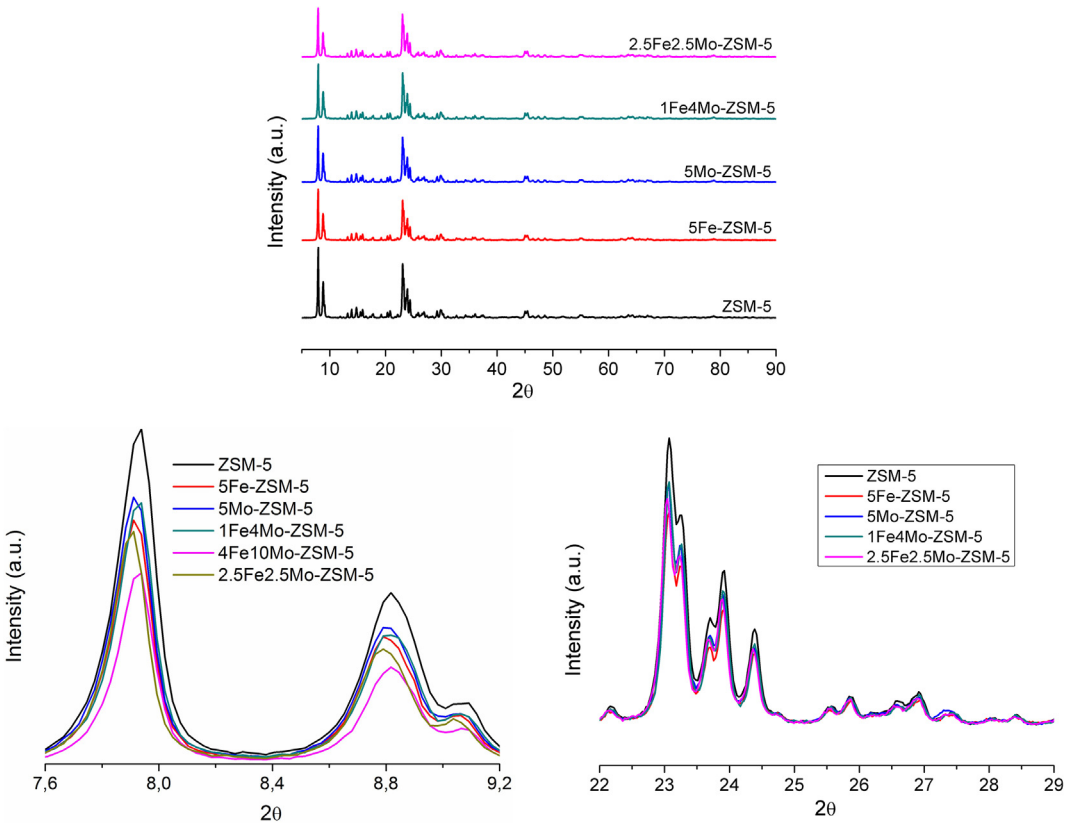

Fig. 7 XRD patterns of the HZSM-5 and 5Fe-, 5Mo-, 1Fe4Mo- and 2.5Fe2.5Mo-ZSM-5 catalysts.

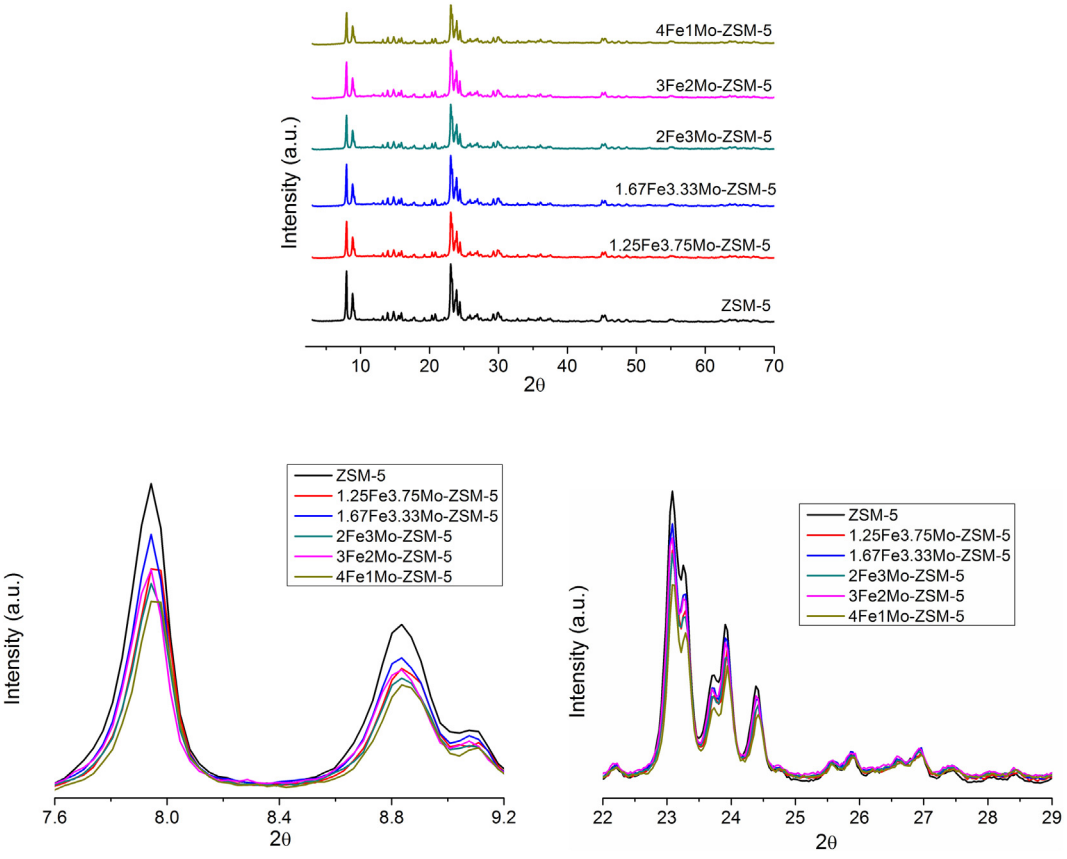

Fig. 8 XRD patterns of the HZSM-5, 1.25Fe3.75Mo-, 1.67Fe3.33Mo-, 2Fe3Mo-, 3Fe2Mo- and 4Fe1Mo-ZSM-5 catalysts.

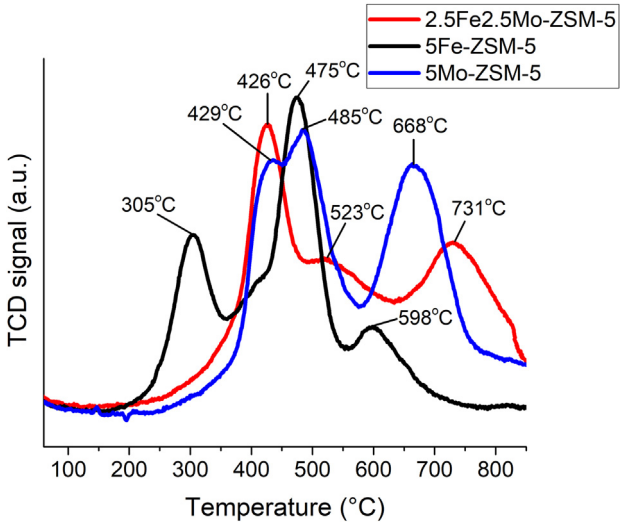

Fig. 9 H_2-TPR profiles of the 5Fe-ZSM-5, 5Mo-ZSM-5 and 2.5Fe2.5Mo-ZSM-5 catalysts.

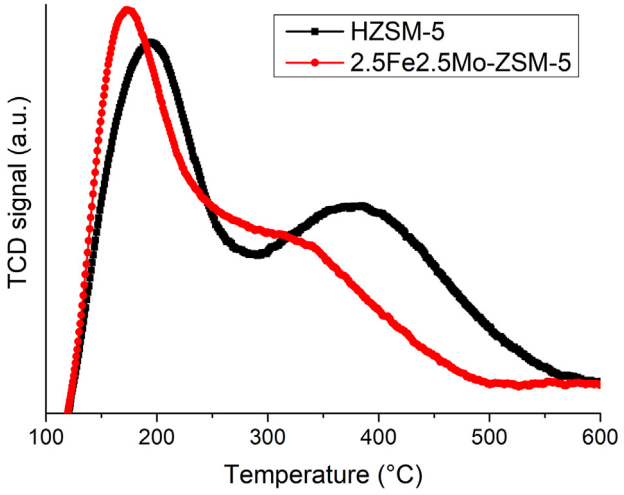

Fig. 10 NH_3-TPD profiles of the HZSM-5 and 2.5Fe2.5Mo-ZSM-5 catalysts.

xFeyMo-ZSM-5 and HZSM-5 catalysts, showing that 1-hexene is a very active feed.

Fig. 11 shows that a high gasoline selectivity (>40%) was observed for the 2.5Fe2.5Mo-ZSM-5 and 3Fe2Mo-ZSM-5 catalysts.

The parent HZSM-5 with other promoted catalysts being kept at 40% and less. The best selectivity for C_6-C_9 was

Table 4 Total acidity expressed as mmol pyridine chemisorbed per gram of catalyst.

Sample	Total acidity, mmol/g_{cat}	BAS/LAS
HZSM-5	0.63	4.0
2.5Fe2.5Mo-HZSM-5	0.58	2.7

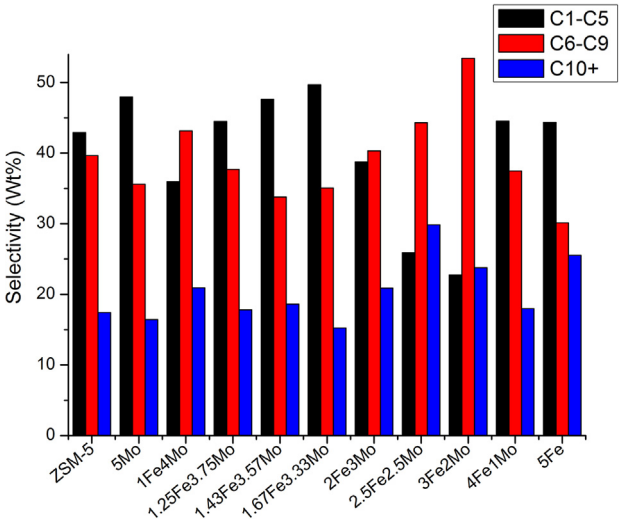

Fig. 11 Effect of Fe/Mo ratio with TOS = 6 h on the selectivity of C_1-C_5, C_6-C_9, C_{10+} hydrocarbons.

obtained over 3Fe2Mo-ZSM-5 catalyst, but C_{10+} (>25%) over 2.5Fe2.5Mo-ZSM-5 and being higher (9wt%) than parent HZSM-5 catalyst after TOS = 6 h.

Fig. 12 shows the product distribution of grouped fractions of C_1-C_{17+} from the liquid product for the HZSM-5, 2.5Fe2.5Mo-ZSM-5 and 3Fe2Mo-ZSM-5 catalysts.

The product distribution of C_8, C_9 and C_{10} was 15.1%, 20.5% and 11.9% respectively for the HZSM-5 catalyst. Upon addition of Fe-Mo to the parent H-ZSM-5 catalyst the product distribution of C_8, C_9 and C_{10} increased to 11.3%, 31.2%, 23.0% for the 2.5Fe2.5Mo-ZSM-5 and 18.9%, 30.4%, 18.2% for the 3Fe2Mo-ZSM-5, respectively.

The strong interaction between the Fe and Mo species in the 2.5Fe2.5Mo-ZSM-5 and 3Fe2Mo-ZSM-5 catalysts was estimated, which resulted in a high chemical value of Mo^{6+} formed in Fe–Mo bimetal oxide system [38]. Moreover, the catalytic performance of xFeyMo-ZSM-5 catalysts is affected by Fe/Mo molar ratio. This molar ratio has a significant influence on the surface acid site density. The main reason for the enhanced activity of the 2.5Fe2.5Mo-ZSM-5 and 3Fe2Mo-ZSM-5 catalysts is related to the modification

Table 3 NH_3-TPD results for the HZSM-5 and 2.5Fe2.5Mo-ZSM-5.

Catalyst	Desorption Temperature (°C)		Acidity by strength (mmol/g)		Strong/weak
	T_1	T_2	Weak	Strong	
H-ZSM-5	191	389	0.481	0.218	0.453
2.5Fe2.5Mo-ZSM-5	171	340	0.468	0.038	0.081

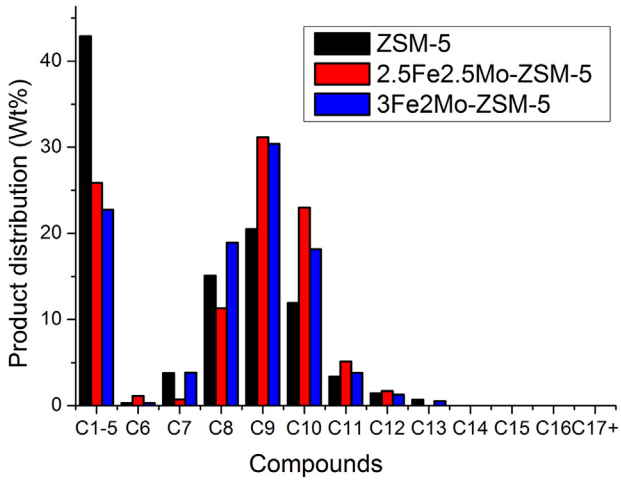

Fig. 12 Product distribution of fuel range hydrocarbons over HZSM-5, 2.5Fe2.5Mo-ZSM-5 and 3Fe2Mo-ZSM-5 samples (TOS = 6 h, T = 350 °C, FR = 0.098 mL/min, WHSV = 4 h^{-1}).

of the acidity H-ZSM-5 resulting in an increase in the Lewis acid sites and a decrease in the BAS/LAS ratio, thus is increased of the selectivity to C_{9+} aromatics what is supported by pyridine-DRIFTS, NH_3-TPD and catalyst evaluation results [18].

The Fe species are important for incorporation to Mo catalyst not only because of their promotional effects and stability but because they are abundant, cheap and environmentally friendly and can have industrial applications [45]. We speculate that the electron transfer (strong interaction) occurred between Fe and Mo species for 2.5Fe2.5Mo-ZSM-5 and 3Fe2Mo-ZSM-5 catalysts and confirmed it by H_2-TPR. Unfortunately, until now no definitive conclusion has been established regarding the effect of Fe additive on Mo catalysts [45], but it can be concluded that the synergetic effect between Fe and Mo species exists and to improve the catalytic performance of 1-hexene aromatization reaction [46].

4. Conclusions

The 1-hexene aromatization was studied on metal modified HZSM-5 and compared with unmodified HZSM-5 (Zeolyst Int., $SiO_2/Al_2O_3 \approx 30$). Modifying of the HZSM-5 catalyst with Fe and Mo species could enhance the rate of aromatics production in the 1-hexene aromatization reaction. At 350 °C, a variety of products were detected, where the C_8 and C_9 were the major products in the gasoline range and C_{10} was the major product in the distillate range. The Fe-Mo modified H-ZSM-5 zeolites were prepared using the incipient wetness impregnation method in a varying ratio. A combination of catalytic testing and detailed catalyst characterization resulted in the identification of effects on the activity depending on the varying ratio of metals in the zeolite catalysts. Adding of the Fe-Mo species to HZSM-5 has been shown to be positive for the high selectivity of gasoline and distillate production both at standard experimental conditions with using atmospheric pressure. The decrease in the amount of strong acid sites results in an increase in the selectivity to C_{9+} aromatics. The 2.5Fe2.5Mo-ZSM-5 and 3Fe2Mo-ZSM-5 catalysts showed higher selectivity in gasoline and distillate range than parent HZSM-5 and others promoted catalysts. Thus, the synergetic effect of Fe and Mo species exists for 2.5Fe2.5Mo-ZSM-5 and 3Fe2Mo-ZSM-5 catalysts, which has improved the catalytic performance of 1-hexene aromatization reaction.

5. Declarations of interest

The authors declare no competing interests.

Acknowledgments

We are grateful to PetroSA for financial support. We are also indebted to Dr. Petar Djinovič (National Institute of Chemistry) for obtaining and description the pyridine-DRIFT spectra of the H-ZSM-5 and 2.5Fe2.5Mo-ZSM-5 samples.

References

[1] Y. Li, S. Liu, Z. Zhang, S. Xie, X. Zhu, L. Xu, Aromatization and isomerization of 1-hexene over alkali-treated HZSM-5 zeolites: Improved reaction stability, Appl. Catal. A Gen. 338 (2008) 100–113, https://doi.org/10.1016/j.apcata.2007.12.026.

[2] L. Zhang, H. Liu, X. Li, S. Xie, Y. Wang, W. Xin, S. Liu, L. Xu, Differences between ZSM-5 and ZSM-11 zeolite catalysts in 1-hexene aromatization and isomerization, Fuel Process. Technol. 91 (2010) 449–455, https://doi.org/10.1016/j.fuproc.2009.12.003.

[3] Y. Li, S. Liu, S. Xie, L. Xu, Promoted metal utilization capacity of alkali-treated zeolite: preparation of Zn/ZSM-5 and its application in 1-hexene aromatization, Appl. Catal. A Gen. 360 (2009) 8–16, https://doi.org/10.1016/j.apcata.2009.02.039.

[4] R.J. Nash, M.E. Dry, C.T. O'Connor, Aromatization of 1-hexene and 1-octene by gallium/H-ZSM-5 catalysts, Appl. Catal. A Gen. 134 (1996) 285–297.

[5] G. Wang, W. Wu, W. Zan, X. Bai, W. Wang, X. Qi, O.V. Kikhtyanin, Preparation of Zn-modified nano-ZSM-5 zeolite and its catalytic performance in aromatization of 1-hexene, Trans. Nonferrous Met. Soc. China 25 (2015) 1580–1586, https://doi.org/10.1016/S1003-6326(15)63761-X.

[6] I. Coleto, M.I. López, R. Roldán, J.P. Gómez, C. Jiménez-Sanchidrián, F.J. Romero-Salguero, Transformation of 1-hexene on Pt supported ZSM-5 zeolite modified with tin, copper or chromium, React. Kinet. Mech. Catal. (2015), https://doi.org/10.1007/s11144-015-0891-7.

[7] G. Bellussi, F. Mizia, V. Calemma, P. Pollesel, R. Millini, Oligomerization of olefins from Light Cracking Naphtha over zeolite-based catalyst for the production of high quality diesel fuel, Microp. Mesopor. Mater. 164 (2012) 127–134, https://doi.org/10.1016/j.micromeso.2012.07.020.

[8] R. Van Grieken, J.M. Escola, J. Moreno, R. Rodríguez, Liquid phase oligomerization of 1-hexene over different mesoporous aluminosilicates (Al-MTS, Al-MCM-41 and Al-SBA-15) and micrometer/nanometer HZSM-5 zeolites, Appl. Catal. A Gen. 305 (2006) 176–188, https://doi.org/10.1016/j.apcata.2006.02.058.

[9] J.P.G. Pater, P.A. Jacobs, J.A. Martens, Oligomerization of hex-1-ene over acidic aluminosilicate zeolites, MCM-41, and silica-alumina co-gel catalysts: a comparative study, J. Catal. 184 (1999) 262–267, https://doi.org/10.1006/jcat.1999.2423.

[10] R. Quann, L. Green, S.A. Tabak, F.J. Krambeck, Chemistry of olefin oligomerization over ZSM-5 catalyst, Ind. Eng. Chem. Res. (1988) 565–570, https://doi.org/10.1021/ie00076a006.
[11] A. Corma, C. Martínez, E. Doskocil, Designing MFI-based catalysts with improved catalyst life for C 3 = and C 5 = oligomerization to high-quality liquid fuels, J. Catal. 300 (2013) 183–196, https://doi.org/10.1016/j.jcat.2012.12.029.
[12] A. De Klerk, Oligomerization of 1-hexene and 1-octene over solid acid catalysts, Ind. Eng. Chem. Res. 44 (2005) 3887–3893, https://doi.org/10.1021/ie0487843.
[13] R. van Grieken, J.M. Escola, J. Moreno, R. Rodríguez, Direct synthesis of mesoporous M-SBA-15 (M = Al, Fe, B, Cr) and application to 1-hexene oligomerization, Chem. Eng. J. 155 (2009) 442–450, https://doi.org/10.1016/j.cej.2009.07.016.
[14] E. Kriván, S. Tomasek, J. Hancsók, Application Possibilities of Zeolite Catalysts in Oligomerization of Light Olefins, Period. Polytech. Chem. Eng. 58 (2014) 149–156, https://doi.org/10.3311/PPch. 7204.
[15] X.B. Li, X.Y. Jiang, Propylene oligomerization to produce diesel fuel on Zr-ZSM-5 catalyst, Chem. Technol. Fuels Oils 49 (2013) 156–164, https://doi.org/10.1007/s10553-013-0427-7.
[16] V. Abdelsayed, D. Shekhawat, M.W. Smith, Effect of Fe and Zn promoters on Mo/HZSM-5 catalyst for methane dehydroaromatization, Fuel 139 (2015) 401–410, https://doi.org/10.1016/j.fuel.2014.08.064.
[17] Y. Xu, Y. Suzuki, Z.G. Zhang, Comparison of the activity stabilities of nanosized and microsized zeolites based Fe-Mo/HZSM-5 catalysts in the non-oxidative CH4 dehydroaromatization under periodic CH4-H2 switching operation at 1073 K, Appl. Catal. A Gen. 452 (2013) 105–116, https://doi.org/10.1016/j.apcata.2012.11.027.
[18] S.S. Masiero, N.R. Marcilio, O.W. Perez-Lopez, Aromatization of methane over Mo-Fe/ZSM-5 catalysts, Catal. Lett. 131 (2009) 194–202, https://doi.org/10.1007/s10562-009-0032-x.
[19] Y. Xu, J. Wang, Y. Suzuki, Z.G. Zhang, Effect of transition metal additives on the catalytic stability of Mo/HZSM-5 in the methane dehydroaromatization under periodic CH 4–H2 switch operation at 1073 K, Appl. Catal. A Gen. 409–410 (2011) 181–193, https://doi.org/10.1016/j.apcata.2011.10.003.
[20] A.J.J. Koekkoek, H. Xin, Q. Yang, C. Li, E.J.M. Hensen, Hierarchically structured Fe/ZSM-5 as catalysts for the oxidation of benzene to phenol, Microp. Mesop. Mater. 145 (2011) 172–181, https://doi.org/10.1016/j.micromeso.2011.05.013.
[21] Y. Yan, S. Jiang, H. Zhang, Efficient catalytic wet peroxide oxidation of phenol over Fe-ZSM-5 catalyst in a fixed bed reactor, Sep. Purif. Technol. 133 (2014) 365–374, https://doi.org/10.1016/j.seppur.2014.07.014.
[22] Y. Wei, P.E. de Jongh, M.L.M. Bonati, D.J. Law, G.J. Sunley, K.P. de Jong, Enhanced catalytic performance of zeolite ZSM-5 for conversion of methanol to dimethyl ether by combining alkaline treatment and partial activation, Appl. Catal. A Gen. 504 (2015) 211–219, https://doi.org/10.1016/j.apcata.2014.12.027.
[23] L. Huang, F. Qin, Z. Huang, Y. Zhuang, J. Ma, H. Xu, W. Shen, Hierarchical ZSM-5 zeolite synthesized by an ultrasound-assisted method as a long-life catalyst for dehydration of glycerol to acrolein, Ind. Eng. Chem. Res. 55 (2016) 7318–7327, https://doi.org/10.1021/acs.iecr.6b01140.
[24] J. Peréz-Ramírez, D. Verboekend, A. Bonilla, S. Abelló, Zeolite catalysts with tunable hierarchy factor by pore-growth moderators, Adv. Funct. Mater. 19 (2009) 3972–3979, https://doi.org/10.1002/adfm.200901394.
[25] H. Liu, S. Yang, J. Hu, F. Shang, Z. Li, C. Xu, J. Guan, Q. Kan, A comparison study of mesoporous Mo/H-ZSM-5 and conventional Mo/H-ZSM-5 catalysts in methane non-oxidative aromatization, Fuel Process. Technol. 96 (2012) 195–202, https://doi.org/10.1016/j.fuproc.2011.12.034.
[26] M. Rostamizadeh, A. Taeb, Highly selective Me-ZSM-5 catalyst for methanol to propylene (MTP), J. Ind. Eng. Chem. 27 (2015) 297–306, https://doi.org/10.1016/j.jiec.2015.01.004.
[27] B. Li, S. Li, N. Li, H. Chen, W. Zhang, X. Bao, B. Lin, Structure and acidity of Mo/ZSM-5 synthesized by solid state reaction for methane dehydrogenation and aromatization, Microp. Mesop. Mater. 88 (2006) 244–253, https://doi.org/10.1016/j.micromeso.2005.09.016.
[28] G. Espinosa, J.M. Dominguez, L. Diaz, C. Angeles, Catalytic behavior of CoMo/ZSM5 catalysts for CS2 conversion, Catal. Today. 148 (2010) 153–159, https://doi.org/10.1016/j.cattod.2009.03.029.
[29] K. Velebná, M. Horňáček, V. Jorík, P. Hudec, M. Čaplovičová, L. Čaplovič, The influence of molybdenum loading on activity of ZSM-5 zeolite in dehydroaromatization of methane, Microp. Mesop. Mater. 212 (2015) 146–155, https://doi.org/10.1016/j.micromeso.2015.04.001.
[30] F. Lai, X. Liu, W. Li, F. Shen, Macrolactonization of methyl 15-hydroxypentadecanoate to cyclopentadecanolide over Mo-Fe/HZSM-5 catalyst, React. Kinet. Mech. Catal. 100 (2010) 407–415, https://doi.org/10.1007/s11144-010-0196-9.
[31] M. Hosseinpour, H. Amiri, S.J. Ahmadi, M.A. Mousavian, The role of supercritical water on the rapid formation of ZSM-5 nanocatalyst, J. Supercrit. Fluids. (2015), https://doi.org/10.1016/j.supflu.2015.06.013.
[32] X. Zhao, L. Wei, S. Cheng, Y. Huang, Y. Yu, J. Julson, Catalytic cracking of camelina oil for hydrocarbon biofuel over ZSM-5-Zn catalyst, Fuel Process. Technol. 139 (2015) 117–126, https://doi.org/10.1016/j.fuproc.2015.07.033.
[33] X. Cheng, P. Yan, X. Zhang, F. Yang, C. Dai, D. Li, X.X. Ma, Enhanced methane dehydroaromatization in the presence of CO2over Fe- and Mg-modified Mo/ZSM-5, Mol. Catal. 437 (2017) 114–120, https://doi.org/10.1016/j.mcat.2017.05.011.
[34] Q. Dong, X. Zhao, J. Wang, M. Ichikawa, Studies on Mo/HZSM-5 Complex Catalyst for Methane Aromatization, J. Nat. Gas Chem. 13 (2004) 36–40. http://www.scopus.com/inward/record.url?eid=2-s2.0-1942519875&partnerID=40&md5=0622b7394ca255e4ce2c92bb13464759.
[35] Z. Li, K.C. Xie, W. Huang, W. Reschetilowski, Molybdenum loaded on HZSM- 50: a catalyst for selective catalytic reduction of nitrogen oxides 158 (2005) 1741–1748.
[36] H.Y. Wang, T.T. Jiao, Z.X. Li, C.S. Li, S.J. Zhang, J.L. Zhang, Study on palm oil hydrogenation for clean fuel over Ni-Mo-W/??-Al2O3-ZSM-5 catalyst, Fuel Process. Technol. 139 (2014) 91–99, https://doi.org/10.1016/j.fuproc.2015.08.004.
[37] K. Van der Borght, V.V. Galvita, G.B. Marin, Ethanol to higher hydrocarbons over Ni, Ga, Fe-modified ZSM-5: Effect of metal content, Appl. Catal. A Gen. 492 (2015) 117–126, https://doi.org/10.1016/j.apcata.2014.12.020.
[38] H. Lan, X. Xiao, S. Yuan, B. Zhang, G. Zhou, Y. Jiang, Synergistic Effect of Mo–Fe Bimetal Oxides Promoting Catalytic Conversion of Glycerol to Allyl Alcohol, Catal. Lett. 147 (2017) 2187–2199, https://doi.org/10.1007/s10562-017-2124-3.
[39] Q. Zhang, K. Qiu, B. Li, T. Jiang, X. Zhang, L. Ma, T. Wang, Isoparaffin production by aqueous phase processing of sorbitol over the Ni/HZSM-5 catalysts: effect of the calcination temperature of the catalyst, Fuel. 90 (2011) 3468–3472, https://doi.org/10.1016/j.fuel.2011.06.046.
[40] T.E. Tshabalala, N.J. Coville, J.A. Anderson, M.S. Scurrell, Dehydroaromatization of methane over Sn–Pt modified Mo/H-ZSM-5 zeolite catalysts: Effect of preparation method, Appl. Catal. A Gen. 503 (2015) 218–226, https://doi.org/10.1016/j.apcata.2015.06.035.
[41] X. Li, D. Han, H. Wang, G. Liu, B. Wang, Z. Li, J. Wu, Propene oligomerization to high-quality liquid fuels over Ni/HZSM-5, Fuel 144 (2015) 9–14, https://doi.org/10.1016/j.fuel.2014.12.005.

[42] H. Long, X. Wang, W. Sun, G. Xiong, K. Wang, Effect of acidity on n-octene reaction over potassium modified nanoscale HZSM-5, Fuel 87 (2008) 3660–3663, https://doi.org/10.1016/j.fuel.2008.06.007.

[43] J. Li, P. Miao, Z. Li, T. He, D. Han, J. Wu, Z. Wang, J. Wu, Hydrothermal synthesis of nanocrystalline H[Fe, Al]ZSM-5 zeolites for conversion of methanol to gasoline, Energy Convers. Manag. 93 (2015) 259–266, https://doi.org/10.1016/j.enconman.2015.01.031.

[44] M. Tamura, K. Shimizu, A. Satsuma, Applied Catalysis A : General Comprehensive IR study on acid / base properties of metal oxides, Applied Catal. A Gen. 433–434 (2012) 135–145, https://doi.org/10.1016/j.apcata.2012.05.008.

[45] A. Sridhar, M. Rahman, S.J. Khatib, Enhancement of Molybdenum/ZSM-5 Catalysts in Methane Aromatization by the Addition of Iron Promoters and by Reduction/Carburization Pretreatment, ChemCatChem. 10 (2018) 2571–2583, https://doi.org/10.1002/cctc.201800002.

[46] Z. Li, K. Xie, W. Huang, W. Reschetilowski, Selective Catalytic Reduction of NOxwith Ammonia over Fe-Mo/ZSM-5 Catalysts, Chem. Eng. Technol. 28 (2005) 797–801, https://doi.org/10.1002/ceat.200500113.